Research Article

Ghada ALMisned, Elaf Rabaa, Duygu Sen Baykal, Esra Kavaz, Erkan Ilik, Gokhan Kilic, Hesham M. H. Zakaly, Antoaneta Ene*, Huseyin Ozan Tekin*

Mechanical properties, elastic moduli, and gamma ray attenuation competencies of some TeO_2–WO_3–GdF_3 glasses: Tailoring WO_3–GdF_3 substitution toward optimum behavioral state range

https://doi.org/10.1515/chem-2022-0290
received January 27, 2023; accepted February 9, 2023

Abstract: We report the mechanical properties, elastic moduli, and gamma ray attenuation properties of some TeO_2–WO_3–GdF_3 glasses. Using the chemical composition of the selected glasses, the dissociation energy per unit volume (G_t) and the packing density (V_t) were calculated. Using the G_t and V_t values, Young's, Shear, Bulk, Longitudinal Modulus, and Poisson's ratio of the glasses are calculated. Next several fundamental gamma ray attenuation properties such as linear and mass attenuation coefficients, half value layer, mean free path, effective atomic number, effective electron density, effective conductivity, exposure, and energy absorption buildup factors are calculated in 0.015–15 MeV energy range. As a consequence of WO_3–GdF_3 substitution, the glass densities are observed in different values. The overall gamma ray attenuation properties are found to be enhanced through WO_3 addition. Moreover, the increasing WO_3 incorporation into glass configuration decreases the overall elastic moduli of glasses. It can be concluded that increasing WO_3 may be a useful tool for enhancing the gamma ray attenuation qualities and decreasing the elastic moduli of TeO_2–WO_3–GdF_3 in situations where a material with versatile mechanical properties is required.

Keywords: mechanical properties, elastic moduli, gamma ray, WO_3, glass shields

*** Corresponding author: Antoaneta Ene,** INPOLDE Research Center, Department of Chemistry, Physics and Environment, Faculty of Sciences and Environment, Dunarea de Jos University of Galati, 47 Domneasca Street, 800008 Galati, Romania, e-mail: Antoaneta.Ene@ugal.ro
*** Corresponding author: Huseyin Ozan Tekin,** Medical Diagnostic Imaging Department, College of Health Sciences, University of Sharjah, Sharjah, 27272, United Arab Emirates; Istinye University, Faculty of Engineering and Natural Sciences, Computer Engineering Department, Istanbul 34396, Turkey, e-mail: tekin765@gmail.com
Ghada ALMisned: Department of Physics, College of Science, Princess Nourah Bint Abdulrahman University, P.O. Box 84428, Riyadh 11671, Saudi Arabia
Elaf Rabaa: Medical Diagnostic Imaging Department, College of Health Sciences, University of Sharjah, Sharjah, 27272, United Arab Emirates
Duygu Sen Baykal: Vocational School of Health Sciences, Istanbul Kent University, Istanbul 34433, Turkey
Esra Kavaz: Department of Physics, Faculty of Sciences, Ataturk University, 25240 Erzurum, Turkey
Erkan Ilik, Gokhan Kilic: Department of Physics, Faculty of Science, Eskisehir Osmangazi University, Eskisehir, 26040, Turkey
Hesham M. H. Zakaly: Institute of Physics and Technology, Ural Federal University, 620002 Ekaterinburg, Russia; Physics Department, Faculty of Science, Al-Azhar University, Assiut 71524, Egypt

1 Introduction

People are exposed to ionizing radiation on a daily basis through natural radiation sources, including radioactive materials found on earth soil, water, and air. In the past years, people relied on man-made iodizing radiation to serve multiple purposes. Man-made sources of ionizing radiation include nuclear power plants, medical treatment and diagnosis, scientific research, and agricultural applications [1–3]. Despite the benefits of radiation use, the risks and dangers cannot be ignored. Depending on the kind and quantity of radiation dose absorbed, radiation may cause serious harm to living biological tissues and sensitive organs. A high dose of radiation may cause erythema, tissue, and skin burns, or even in extreme cases, death [4,5]. In addition to other situations, exposure to constant radiation may cause cancer and other

Open Access. © 2023 the author(s), published by De Gruyter. This work is licensed under the Creative Commons Attribution 4.0 International License.

chromosomal abnormalities. Ionizing radiation is known to induce direct and indirect harm to living tissues by disrupting cell structure and damaging genetic information (DNA) [6]. Therefore, the fundamental use of radiation shielding is a must to provide safety to people and the environment from radiation risks. Medical personnel and patients are frequently exposed to radiation, requiring commitment to radiation protection guidelines and principles (ALARA), such as reducing exposure duration and increasing distance from the radiation source, as well as providing radiation shielding to prevent contact with radiation source energy. Typically, traditional lead (Pb) and some other materials may be incorporated as protective structures into clothes, gloves, aprons, shielded glasses, etc. [7–9]. However, due to the drawbacks of Pb and other conventional protection materials, researchers have moved their focus to glass materials due to its transparency, high thermal and chemical stability, non-toxicity, and high durability, which make them a good alternative option as a shielding material for radiation protection purposes [10–14]. Many types of glass materials have been investigated in respect of their gamma ray attenuation qualities and suitability for such applications, according to the literature review. Among the glass types, tellurite glass is a glass-forming oxide, as it occurs in a wide range of compositions in a variety of applications due to its non-crystalline nature, as also known by its low melting point and the lack of hygroscopic qualities [11,15,16]. It became widespread in photonics technologies and in associated fields by the fact of its high density and low transition temperature [17]. Their optical properties have gained the researchers interest, including high refractive and non-linear index, high dielectric constant, in addition to its high chemical stability and transmission of wide range of infrared [18]. When employing tellurite as a composition with other materials, it not only improved the glass-forming ability but also the thermal stability [19]. In all cases, when TeO_2 was used as a glass-forming agent, its concentration was generally the highest, while the other oxide materials being as a modified agent [20,21]. According to a number of published studies, the addition of WO_3 to tellurite glasses synergistically improves a number of parameters, including the quantity of gamma absorption [22–24]. This wide scientific interest pushed us to look into the differences in gamma ray absorption properties as a function of the stages in which WO_3 is doped at different rates into tellurite glasses and GdF_3 is added as a modifier at different rates [25]. Moreover, in our study, tellurite was the first and dominant component, while the second component GdF_3 was chosen as a modifier due to its high density, high transmittance, and ability to provide high stability, all of which would improve the glass network. GdF_3 is widely used as a host in fluorescent materials, as well as the selection of fluoride would improve the glass system's anti-crystallization abilities. The third component of the glass is WO_3, while it is a glass former it would not only improve the glass transition temperature but also would maintain the high density and refraction index. The detailed outcomes of this research may assist in understanding the absorption properties of WO_3-doped tellurite glasses modified through GdF_3. Furthermore, the findings of this research may lead to a comprehensive assessment of similar glass mixtures reported in the scientific literature, therefore simplifying the application of the optimum useful configurations in the radiation protection process employing glass shields.

2 Materials and methods

In this section of the investigation, we have gathered crucial information about the gamma radiation shielding capabilities of four TeO_2–WO_3–GdF_3 glass samples [25]. The four glass samples were previously prepared using the traditional method of melt-quenching, each sample S1, S2, S3, and S4 had a unique composition in order to identify various densities for evaluating gamma ray absorption qualities between 0.015 and 15 MeV.

2.1 Gamma ray attenuation properties

Py-MLBUF software [26] was used to estimate the gamma ray absorption characteristics of each prepared glass sample, and ORIGIN software was afterwards utilized to demonstrate the findings in detail. In this study, the mass attenuation coefficient, linear attenuation coefficient (μ), half value layer (HVL) have been calculated and reported. In addition, several critical data such as mean free path (mfp), effective electron conductivity (C_{eff}), effective electron density (N_{eff}), and effective atomic number (Z_{eff}) were collected to assess the efficiency of the shielding for a variety of photon energies from 0.015 MeV to 15 MeV, respectively. Moreover, two crucial buildup factors such as exposure (EBF) and energy absorption (EABF) were extensively determined in 0.015–15 MeV range for different mfp values to assess the ratio of collided and un-collided photon during the photon–matter interaction process as a function of glass configuration. As seen in Table 1, four different

Table 1: Four different proportions of TeO_2–WO_3–GdF_3 glass system with their density values

Sample code	mol%	Density (g/cm^3)
S1	TeO_2 (70%)–WO_3 (0%)–GdF_3 (30%)	5.4381
S2	TeO_2 (70%)–WO_3 (10%)–GdF_3 (20%)	5.4950
S3	TeO_2 (70%)–WO_3 (30%)–GdF_3 (0%)	5.5082
S4	TeO_2 (70%)–WO_3 (20%)–GdF_3 (10%)	5.5113

proportions of TeO_2–WO_3–GdF_3 glass system have been listed along with their density (g/cm^3) values. The composition of TeO_2 has by far the greatest mol% of 70, while the mol% of GdF_3 and WO_3 were varied from 0 to 30% to study various densities and determine the optimal optical and physical qualities for radiation protection purposes. Through our prior investigations [27,28], as well as other published materials [29,30], one could collect additional specific data and theoretical calculation methodologies about these identified important factors for mechanical properties, elastic moduli, as well as gamma ray attenuation parameters.

2.2 Mechanical properties and elastic moduli

Mechanical properties of TeO_2–WO_3–GdF_3 glasses were obtained by Makishima and Mackenzie model [31]. With the help of the chemical composition of the selected glasses, the dissociation energy per unit volume (G_t) and the packing density (V_t) were calculated. Using the G_t and V_t values, Young's modulus (Y), Shear modulus (G), Bulk modulus (K), Longitudinal modulus (L), and Poisson's ratio (σ) of the glasses were calculated using the following expressions [32,33];

$$V_t = \frac{1}{V_m}\sum_i x_i V_i, \tag{1}$$

$$V_i = N_A\left(\frac{4\pi}{3}\right)(xR_A^3 + yR_O^3), \tag{2}$$

$$Y = 9.38 V_t G_t \quad \text{(GPa)}, \tag{3}$$

$$K = 10 V_t^2 G_t \quad \text{(GPa)}, \tag{4}$$

$$G = \frac{30 V_t^2 G_t}{(10.2 V_t - 1)} \quad \text{(GPa)}, \tag{5}$$

$$L = K + \left(\frac{4G}{3}\right) \quad \text{(GPa)}, \tag{6}$$

$$\sigma = \frac{Y}{2G} - 1, \tag{7}$$

where R_O and R_A are the ionic radius of oxygen and metal, respectively.

3 Results and discussion

3.1 Gamma ray attenuation properties of investigated glasses

The gamma ray absorption properties of four distinct compositions of the TeO_2–WO_3–GdF_3 glass system were investigated in this work. Separately, gamma ray absorption characteristics were evaluated via a sophisticated calculation Py-MLBUF program [26]. Ionizing gamma and X-ray absorption materials often have similarities in density and absorption properties. High-density materials are more efficient in absorbing this kind of radiation because the incident radiation is more likely to be absorbed via internal interactions and to interact with more electrons [34]. Using fundamental calculations, differences in gamma ray attenuation qualities as a function of analyzed glass structure have been determined. The linear attenuation coefficient, also known as μ, is a density-dependent parameter of a certain absorber material. Using the Beer–Lambert equation, one can calculate the μ value using the following equation:

$$I = I_0 \cdot e^{-\mu x}, \tag{8}$$

where I_0 represents the intensity of the incoming beam, I represent the intensity of the beam after transmission through a thickness of x (cm), and μ represents the absorption coefficient (cm^{-1}) of the attenuator sample [35]. Figure 1 depicts the physical appearance of a gamma ray transmission setup, where the abovementioned parameters can be observed. Meanwhile, each of the four glass samples displayed various densities. High density

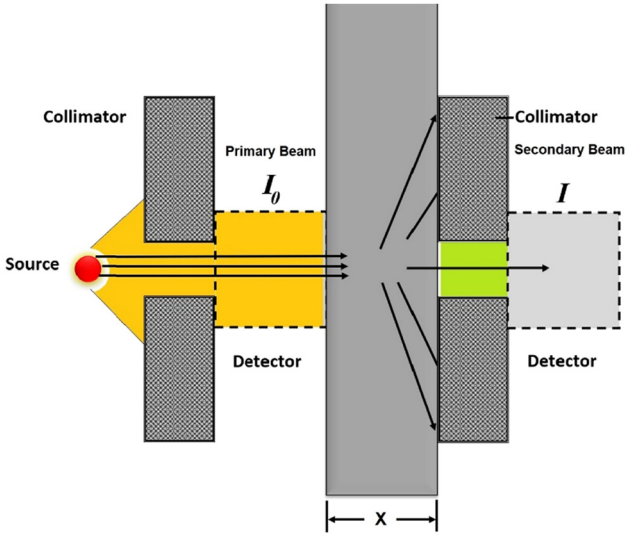


Figure 1: A typical setup for calculation of linear attenuation coefficients.

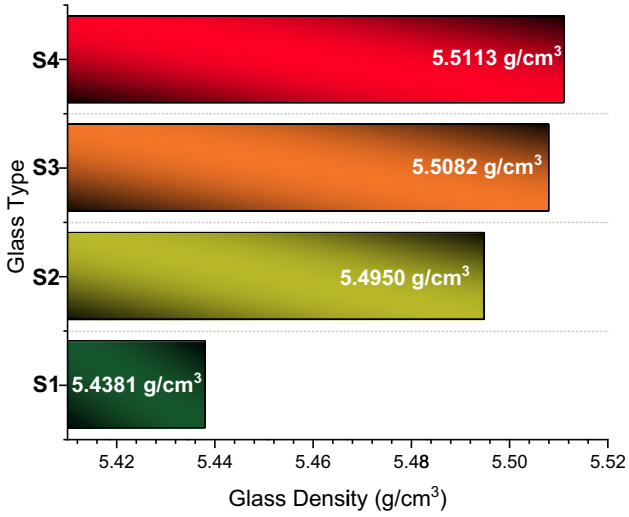


Figure 2: Variation in investigated glass densities (g/cm^3).

is an essential parameter in radiation shielding studies, this means that a material is having more atoms and electrons per unit volume, which would make the material ideal for blocking gamma rays, due to the high probability of interaction that would increase the shielding effects. As seen in Figure 2, a considerable density difference exists between S1 and S4 samples. However, a small difference was found between S4, which contains 70 mol% TeO_2, 20 mol% WO_3, and 10 mol% GdF_3, and S3, which contains 70 mol% TeO_2 and 30 mol% WO_3, resulting in a density of 5.5113 (g/cm^3) and 5.5082 (g/cm^3). These adjacent densities would be explained by the high concentration of WO_3 in sample S3, while the addition of GdF_3 in S4 sample has encouraged to build up the structure, resulting in the maximum density of the glass samples. The measurement of gamma ray absorption properties as a function of density change in the glass system would be affected by the contribution of WO3. Figure 3 shows the relationship between incident energy and the linear attenuation coefficients (cm^{-1}) for the four tested materials (MeV). This fluctuation consequently represents the behavior of the incoming photon energy as it is absorbed or deflected by various interactions such as Compton scattering and the photoelectric effect [36]. As the energy increases, the effect of Compton scattering increases as well, where a part of a photon's energy is transferred to an electron in the shielding material, contributing to a reduction in the linear attenuation values at an energy of 0.05–5 MeV. A rapid decline appeared in the graph in energy from 0.04 to 8 MeV. However, our result proved that S4 with the high WO_3 concentration sample along with 10 mol% GdF_3 had the highest value of all the samples with a 77.9 cm^{-1} at 0.04 MeV as seen in Figure 3. In addition, density-independent parameter MAC is an additional crucial quantity for understanding the partial absorption, which results in the removal of the incoming gamma ray per unit mass [37–39]. Figure 4 demonstrates that S4 with the large composition of WO_3 sample has the highest value in the low energy range, while it decreases to become the lowest value of 0.0406 cm^2/g at 1 MeV. HVL values are indicated in Figure 5 which represent the thickness of the material samples needed to reduce the incident photon energy to half. To determine the optimal material sample, the thickness needed should be as low as possible. There is a direct relationship between photon energy and HVL, as the energy increases, the HVL values increases as well. S4 with high WO_3 composition structure is proven to have the lowest HVL values compared to the rest of the glass samples. For instance, HVL values were reported as 3.275 cm, 3.1916 cm, 3.1395 cm, and 3.0999 cm for S1, S2, S4, and, S4, respectively at 15 MeV energy value. The inverse connection between linear attenuation level and HVL successfully explains the behavior of the S4 sample under these investigation parameters. In addition, a common calculation of the mfp is done, which shares the same concept as the HVL; however, it is defined as the average distance between the two adjacent photon interaction within the absorber material. Low mfp is a good attenuation indicator, which explains that interactions occurred at a short range. As seen in Figure 6, with the increase in the energy, S4 sample is proven to have the lowest mfp value compared to the rest of the sample's due to the positive effect of WO_3 composition in gamma ray absorption properties. Furthermore, effective atomic

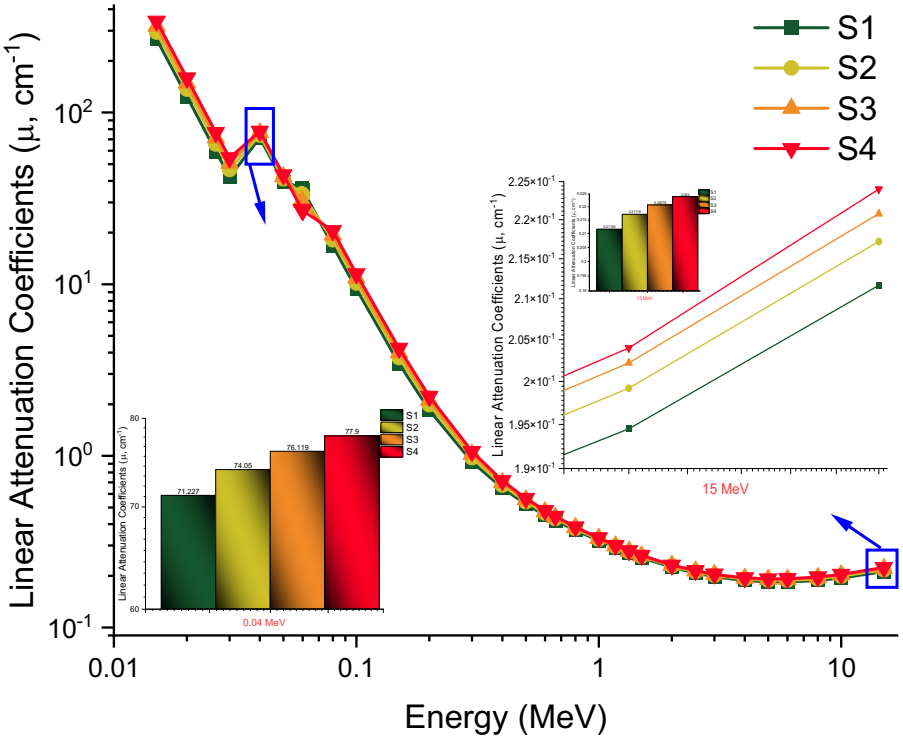


Figure 3: Variation in linear attenuation coefficient (cm^{-1}) with photon energy (MeV) for all S1–S4 glasses.

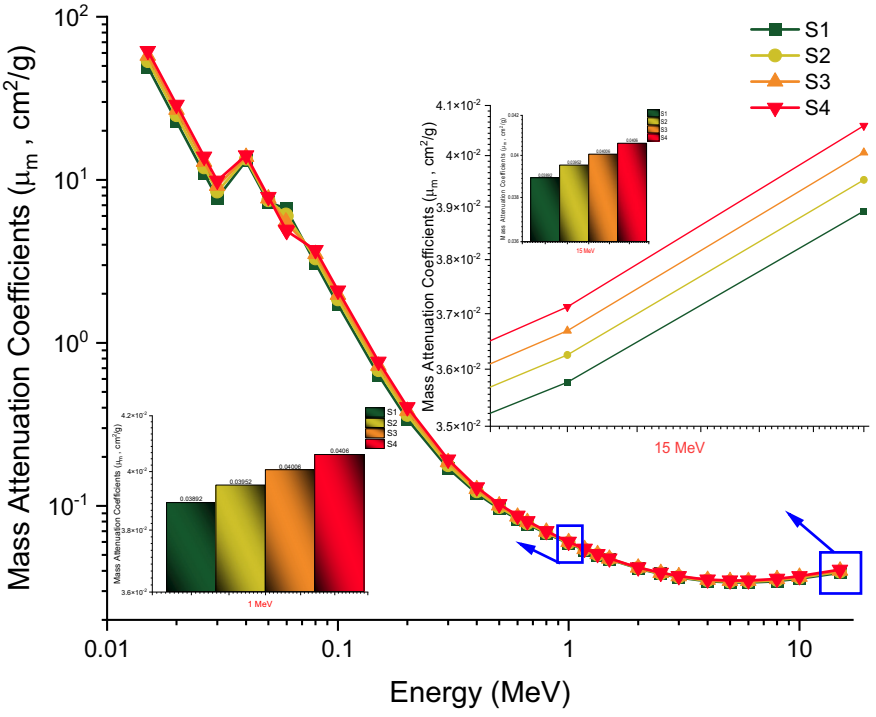


Figure 4: Variation in mass attenuation coefficients (cm^2/g) with photon energy (MeV) for all S1–S4 glasses.

number (Z_{eff}) is one of the important radiation absorption parameters, which is related with the number of electrons in the atom orbit [40,41]. Therefore, the larger the number, the greater the collision with the atomic electron, resulting

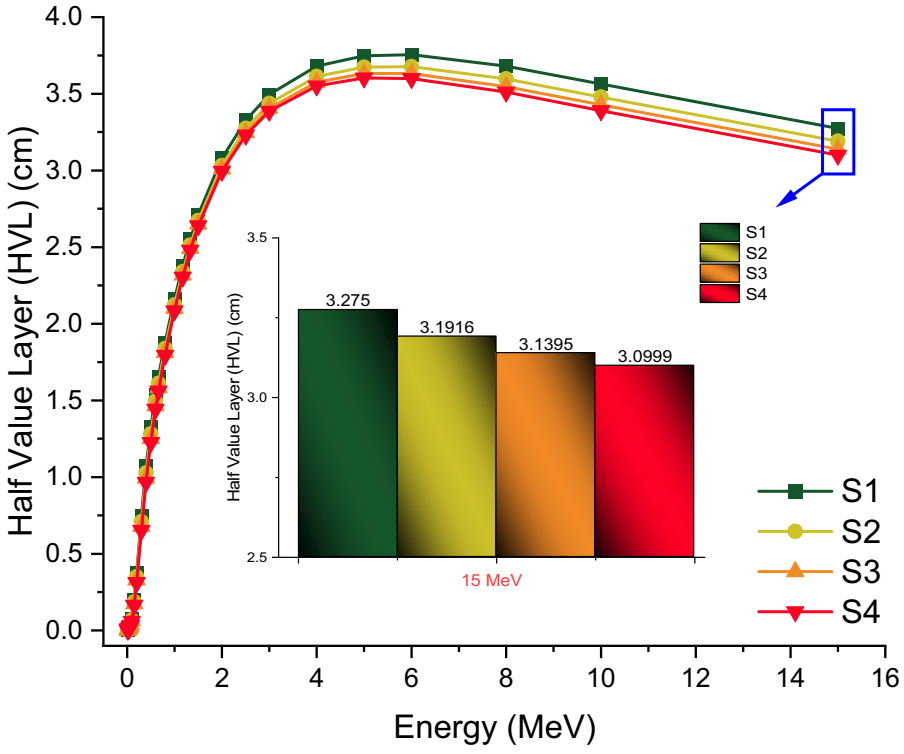


Figure 5: Variation in half value layer (cm) with photon energy (MeV) for all S1–S4 glasses.

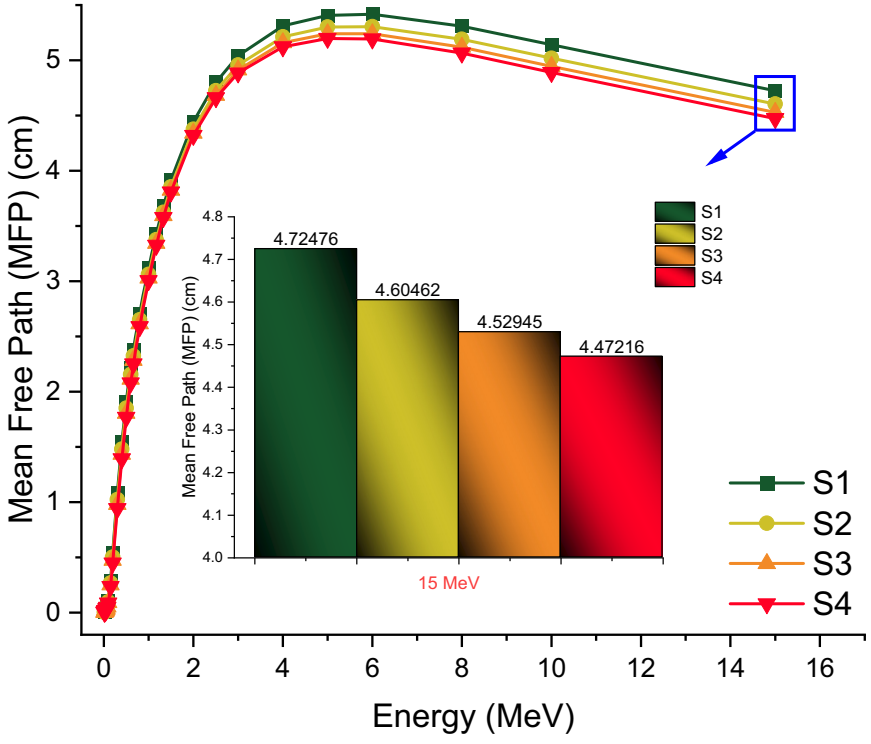


Figure 6: Variation in mfp (cm) with photon energy (MeV) for all S1–S4 glasses.

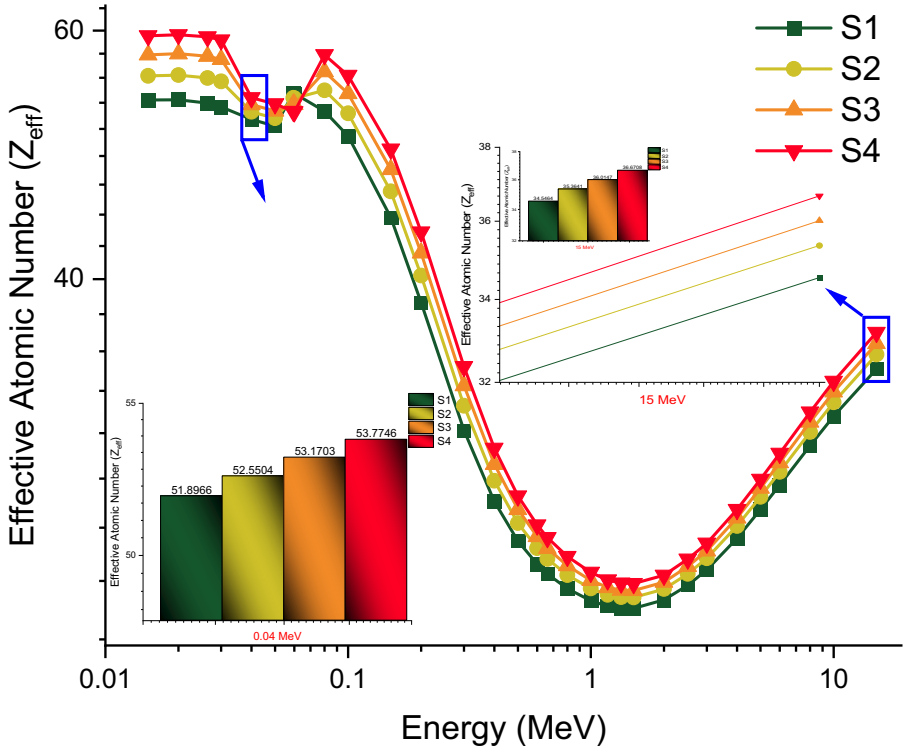


Figure 7: Variation in effective atomic number (Z_{eff}) with photon energy (MeV) for all S1–S4 glasses.

in a high absorption percentage due to the release of energy in every collision of the incoming photon. Figure 7 shows a rapid decline mainly where Compton scattering effect is dominant, and S4 with the 20 mol% WO_3 and 10 mol%

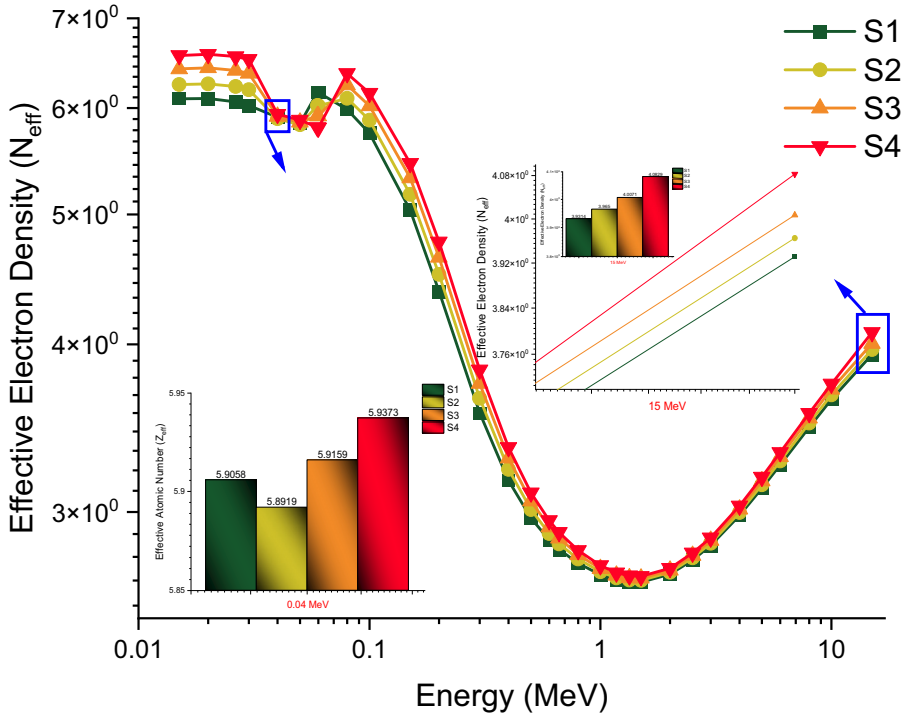


Figure 8: Variation in effective electron density (electrons/g) with photon energy (MeV) for all S1–S4 glasses.

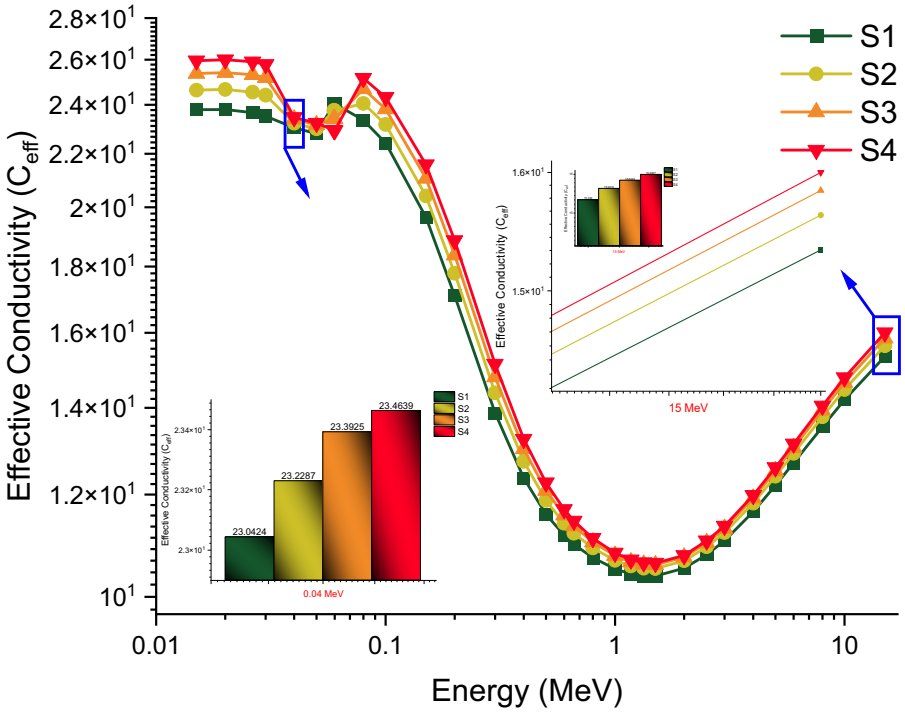


Figure 9: Variation in effective conductivity (C_{eff}) with photon energy (MeV) for all S1–S4 glasses.

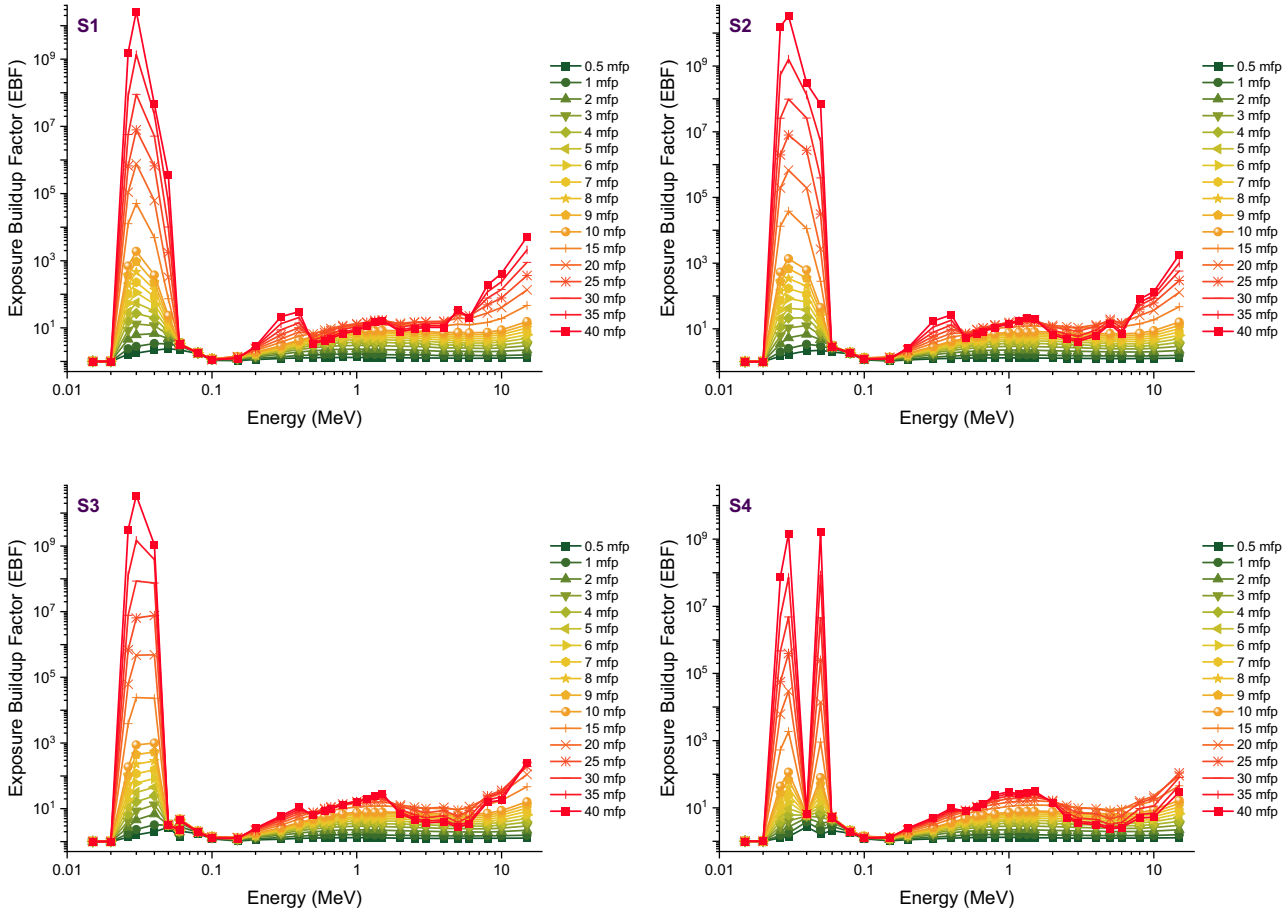


Figure 10: Variation in EBFs of investigated glasses at different mfp values.

GdF_3 is reported with the highest (Z_{eff}) at all energies in the utilized range (i.e., 0.015–15 MeV). For example, Z_{eff} values were reported as 51.8966, 52.5504, 53.1703, and 53.7746 for S1, S2, S3, and S4, respectively, at 0.04 MeV photon energy. Meanwhile, effective conductivity (C_{eff}) and electron density (N_{eff}) are proportional to each other. Figure 8 shows the variation in effective electron density in the S1, S2, S3, and S4 glass samples. Effective electron density is normally at its highest value in low energy range, as it decreases when the energy starts to increase, especially when photoelectric effect becomes dominant. Among all glass samples, S4 sample with 30 mol% WO_3 and 10 mol% GdF_3, had the greatest electron density of all glass samples, making it the sample with the highest effective conductivity (C_{eff}) as well, with a value of 25.1652 (C_{eff}) at 0.08 MeV. The buildup parameter is a crucial element in nuclear physics and radiation shielding calculations in particular. Due to a rise in radiation absorption, this number may approach minimum values. The fluctuation of determined EBF and EABF values for S1, S2, S3, and S4 glasses containing various amounts of TeO_2, WO_3, and GdF_3 at various mfp values from 0.5 to 40 is seen in Figures 9 and 10, respectively. As seen by the graphs, EBF and EABF levels have reached a minimum at low mfp values. This demonstrates the excess rate of photon interactions that the main photon experiences after its penetration into the absorber material. As the mfp value increased, the EBF and EABF numbers increased as well. This circumstance begins with the material's introduction and continues onwards. Figures 9 and 10 also demonstrate that the EBF and EABF values of the sample with low WO_3 incorporation are much greater than those of the sample with 20 mol% WO_3 and 10 mol% GdF_3 in glass configuration. This indicates that the number of photon interactions in 20 mol% WO_3 and 10 mol% GdF_3 doped glass is considerable. The great number of interactions is indeed a crucial indicator that the quantitative absorption process may move ahead at a faster rate, as is well-known. Among the examined glass samples, S4 was determined to have the optimal composition for absorbing energetic gamma rays along with the lowest EBF and EABF values that are crucial markers for maximum photon–matter interaction inside the absorber. This analysis was conducted to determine the optimal radiation shielding

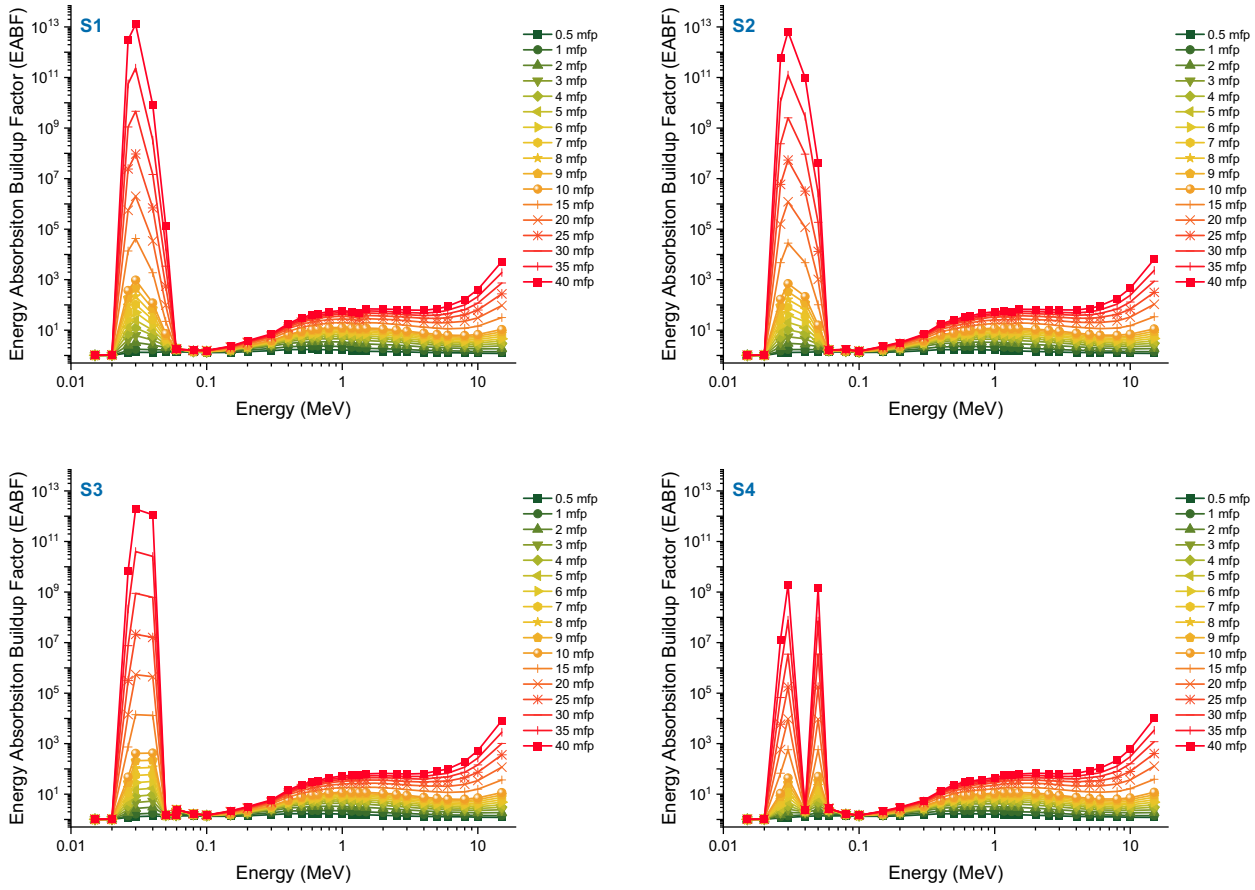


Figure 11: Variation in EABF of investigated glasses at different mfp values.

Table 2: Mechanical properties of the investigated glasses

Sample code	Makishima-Mackenzie model (MMM)							
	g/mol MV	V_t	G_t	Young's modulus Y (GPa)	Bulk modulus K (GPa)	Shear modulus G (GPa)	Longitudinal modulus L (GPa)	Poisson's σ
S1	32.361	0.502	16.391	68.839	41.367	30.091	81.488	0.224
S2	32.341	0.507	15.564	65.971	40.012	28.773	78.376	0.226
S3	32.893	0.507	13.909	58.965	35.767	25.717	70.056	0.226
S4	32.560	0.508	14.736	62.578	38.022	27.281	74.398	0.227

properties for the four glass samples; however, S4 exhibited the maximum material density, yet the same sample with 20 mol% WO_3 and 10 mol% GdF_3 demonstrated considerable radiation shielding properties upon all materials samples, making it suitable for attenuating gamma radiation and to provide shielding against ionizing radiation. Overall, our analysis of the absorption properties of intense photons revealed that they are consistent. As 30 mol% WO_3 + 10 mol% GdF_3 doped glass (i.e., S4) has been determined to have the optimal composition for absorbing gamma rays among the glass samples examined (Figure 11).

3.2 Mechanical properties of investigated glasses

As a result of the calculations, the changes in elastic properties due to the increased WO_3 contribution for TeO_2–WO_3–GdF_3 glasses according to the Makishima-Mackenzie model were examined. Table 2 presents the elastic modulus findings depending on the variation in WO_3–GdF_3 concentrations of glasses. The Young's modulus (Y) found ranged from 68.83 to 58.96 GPa, the longitudinal modulus (L) and mass modulus (K) ranged from 81.48 to 70.05 GPa and 41.36 to 35.76 GPa, respectively. The shear modulus (S) decreased from 30.09 to 25.71 (GPa), while the Poisson ratio (σ) was found to be between 0.224 and 0.227. The replacement of WO_3 with GdF_3 decreased the total elastic modulus of the glass network. This is because the coordination index of W is lower than that of Gd. It is evident that the elastic modulus of glasses is affected by the atomic matrix' looseness or density.

4 Conclusion

Due to the drawbacks of lead and other conventional protection materials, researchers have moved their focus to glass system materials due to its transparency, high thermal and chemical stability, non-toxicity, and high durability, which make it a good alternative option for radiation protection. Our goal in this study is to investigate the radiation shielding properties of four glass samples containing TeO_2–WO_3–GdF_3 in varying amounts. Four glass samples of tellurite, tungsten(VI) oxide, and gadolinium fluoride have been designed using conventional melt-quenching process. Each sample of S1, S2, S3, and S4 were made with different composition in order to determine the distinct densities for studying the gamma ray absorption properties in the range of 0.015–15 MeV. S4 with 70 mol% TeO_2, 20 mol% WO_3, and 10 mol% GdF_3 had the highest density of all samples, due to the high composition of WO_3 that have advanced the glass structure qualities. S4 sample, which showed the highest linear absorption coefficient values among the examined glass materials, was reported as the sample with the lowest values among the HVL values. For example, HVL values for S1, S2, S3, and S4 samples were obtained as 3.275 cm, 3.1916 cm, 3.1395 cm, and 3.0999 cm, respectively. On the other hand, S3 with 30% WO_3 sample proved to have the lowest mfp value compared to the rest of the samples due to the positive effect of WO_3 composition in gamma ray absorption properties, yet with a decreasing effect on the total elastic modulus. It can be concluded that increasing WO_3 may be a useful tool for enhancing the gamma ray attenuation qualities and decreasing the elastic moduli of TeO_2–WO_3–GdF_3 in situations where a material with versatile mechanical properties is required.

Acknowledgements: The authors would like to express their deepest gratitude to Princess Nourah Bint Abdulrahman University Researchers Supporting Project number (PNURSP2023R149), Princess Nourah Bint Abdulrahman University, Riyadh, Saudi Arabia.

Funding information: Princess Nourah Bint Abdulrahman University Researchers Supporting Project number (PNU RSP2023R149), Princess Nourah Bint Abdulrahman University, Riyadh, Saudi Arabia.

Author contributions: H.O.T. – conceptualization, writing – original draft, supervision, and writing – review and editing; G.A. – visualization, software, and writing – original draft; H.M.H.Z. – formal analysis and data curation; E.K. – data curation, formal analysis, and writing – original draft; G.K. – data curation, formal analysis, and writing – original draft; E.I. – data curation, formal analysis, and writing – original draft; D.S.B. – visualization and software; M.S.A. – visualization and software; A.E. – methodology and funding acquisition (The author A.E. would like to thank "Dunarea de Jos" University of Galati, Romania, for the material and technical support).

Conflict of interest: None.

Data availability statement: The datasets generated during and/or analyzed during the current study are available from the corresponding author on reasonable request.

Ethical approval: The conducted research is not related to either human or animal use.

References

[1] Abdelaziz YA, Salama S, Mahmoud R. Outlines on protection of workers from ionizing radiations. J Nucl Technol Appl Sci. 2021;9(1):63–75. doi: 10.21608/jntas.2021.87604.1044.

[2] Singh VK, Pollard HB. Ionizing radiation-induced altered microRNA expression as biomarkers for assessing acute radiation injury. Expert Rev Mol diagnostics. 2017;17(10):871–4. doi: 10.1080/14737159.2017.1366316.

[3] Abd El-Rehim HA. Characterization and possible agricultural application of polyacrylamide/sodium alginate crosslinked hydrogels prepared by ionizing radiation. J Appl Polym Sci. 2006;101(6):3572–80. doi: 10.1002/app.22487.

[4] Mendelsohn FA, Divino CM, Reis ED, Kerstein MD. Wound care after radiation therapy. Adv skin wound care. 2002;15(5):216–24. https://journals.lww.com/aswcjournal/Fulltext/2002/09000/Wound_Care_After_Radiation_Therapy.7.aspx.

[5] Nénot JC. Radiation accidents over the last 60 years. J Radiol Prot. 2009;29(3):301. doi: 10.1088/0952-4746/29/3/R01.

[6] Desouky O, Ding N, Zhou G. Targeted and non-targeted effects of ionizing radiation. J Radiat Res Appl Sci. 2015;8(2):247–54. doi: 10.1016/j.jrras.2015.03.003.

[7] Schmid E, Panzer W, Schlattl H, Eder H. Emission of fluorescent x-radiation from non-lead based shielding materials of protective clothing: A radiobiological problem. J Radiol Prot. 2012;32(3):N129. doi: 10.1088/0952-4746/32/3/N129.

[8] McCaffrey JP, Shen H, Downton B, Mainegra-Hing E. Radiation attenuation by lead and nonlead materials used in radiation shielding garments. Med Phys. 2007;34(2):530–7. doi: 10.1118/1.2426404.

[9] Almurayshid M, Alsagabi S, Alssalim Y, Alotaibi Z, Almsalam R. Feasibility of polymer-based composite materials as radiation shield. Radiat Phys Chem. 2021;183:109425. doi: 10.1016/j.radphyschem.2021.109425.

[10] ALMisned G, Bilal G, Baykal DS, Ali FT, Kilic G, Tekin HO. Bismuth (III) oxide and boron (III) oxide substitution in bismuth-boro-zinc glasses: A focusing in nuclear radiation shielding properties. Optik. 2023;272:170214. doi: 10.1016/j.ijleo.2022.170214.

[11] Kilic G, Ilik E, Issa SA, ALMisned G, Tekin HO. ZnO/CdO translocation in P_2O_5-TeO_2-ZnO ternary glass systems: A reformative enhancement tool for physical, optical, and heavy-charged particles attenuation properties. Optik. 2022;268:169807. doi: 10.1016/j.ijleo.2022.169807.

[12] Alharshan GA, Alrowaili ZA, Olarinoye IO, Sriwunkum C, Tonguc BT, Al-Buriahi MS. Optical borophosphate glass system with excellent properties for radiation shielding applications. Optik. 2022;266:169568. doi: 10.1016/j.ijleo.2022.169568.

[13] AbuAlRoos NJ, Amin NAB, Zainon R. Conventional and new lead-free radiation shielding materials for radiation protection in nuclear medicine: A review. Radiat Phys Chem. 2019;165:108439. doi: 10.1016/j.radphyschem.2019.108439.

[14] Kaundal RS. Comparative study of radiation shielding parameters for bismuth borate glasses. Mater Res. 2016;19:776–80. doi: 10.1590/1980-5373-MR-2016-0040.

[15] Kavaz E, Ilik E, Kilic G, ALMisned G, Tekin HO. Synthesis and experimental characterization on fast neutron and gamma-ray attenuation properties of high-dense and transparent Cadmium oxide (CdO) glasses for shielding purposes. Ceram Int. 2022;48(16):23444–51. doi: 10.1016/j.ceramint.2022.04.338.

[16] Kosuge T, Benino Y, Dimitrov V, Sato R, Komatsu T. Thermal stability and heat capacity changes at the glass transition in K_2O–WO_3–TeO_2 glasses. J Non-Cryst Solids. 1998;242(2–3):154–64. doi: 10.1016/S0022-3093(98)00800-X.

[17] Zhu D, Ray CS, Zhou W, Day DE. Glass transition and fragility of Na_2O–TeO_2 glasses. J Non-Cryst solids. 2003;319(3):247–56. doi: 10.1016/S0022-3093(02)01968-3.

[18] Gupta N, Kaur A, Khanna A, Gonzàlez F, Pesquera C, Iordanova R, et al. Structure-property correlations in TiO_2-Bi_2O_3-B_2O_3-TeO_2 glasses. J Non-Cryst Solids. 2017;470:168–77. doi: 10.1016/j.jnoncrysol.2017.05.021.

[19] Upender G, Vardhani CP, Suresh S, Awasthi AM, Mouli VC. Structure, physical and thermal properties of WO_3–GeO_2–TeO_2 glasses. Mater Chem Phys. 2010;121(1–2):335–41. doi: 10.1016/j.matchemphys.2010.01.050.

[20] Kilic G, Ilik E, Issa SA, Issa B, Al-Buriahi MS, Issever UG, et al. Ytterbium (III) oxide reinforced novel TeO_2–B_2O_3–V_2O_5 glass system: Synthesis and optical, structural, physical and thermal properties. Ceram Int. 2021;47(13):18517–31. doi: 10.1016/j.ceramint.2021.03.175.

[21] Silva MAP, Messaddeq Y, Ribeiro SJL, Poulain M, Villain F, Briois V. Structural studies on TeO_2–PbO glasses. J Phys Chem Solids. 2001;62(6):1055–60. doi: 10.1016/S0022-3697(00)00278-X.

[22] Issa SA, Rashad M, Hanafy TA, Saddeek YB. Experimental investigations on elastic and radiation shielding parameters of WO_3-B_2O_3-TeO_2 glasses. J Non-Cryst Solids. 2020;544:120207. doi: 10.1016/j.jnoncrysol.2020.120207.

[23] Kozlovskiy A, Shlimas DI, Zdorovets MV, Popova E, Elsts E, Popov AI. Investigation of the Efficiency of Shielding Gamma and Electron Radiation Using Glasses Based on TeO_2-WO_3-Bi_2O_3-MoO_3-SiO to Protect Electronic Circuits from the Negative Effects of Ionizing Radiation. Materials. 2022;15(17):6071. doi: 10.3390/ma15176071.

[24] El-Denglawey A, Issa SA, Saddeek YB, Elshami W, Sayed MA, Elsaman R, et al. Mechanical, structural and nuclear radiation shielding competencies of some tellurite glasses reinforced with molybdenum trioxide. Phys Scr. 2021;96(4):045702. doi: 10.1088/1402-4896/abe1f8.

[25] Li C, Zhang X, Onah VC, Yang W, Leng Z, Han K, et al. Physical and optical properties of TeO_2–WO_3–GdF_3 tellurite glass system. Ceram Int. 2022;48(9):12497–505. doi: 10.1016/j.ceramint.2022.01.116.

[26] Mann KS, Mann SS. Py-MLBUF: Development of an online-platform for gamma-ray shielding calculations and investigations. Ann Nucl Energy. 2021;150:107845. doi: 10.1016/j.anucene.2020.107845.

[27] Tekin HO, ALMisned G, Susoy G, Ali FT, Baykal DS, Ene A, et al. Transmission factor (TF) behavior of Bi_2O_3–TeO_2–Na_2O–TiO_2–ZnO glass system: A Monte Carlo simulation study. Sustainability. 2022;14(5):2893. doi: 10.3390/su14052893.

[28] ALMisned G, Baykal DS, Susoy G, Kilic G, Zakaly HM, Ene A, et al. Determination of gamma-ray transmission factors of WO_3–TeO_2–B_2O_3 glasses using MCNPX Monte Carlo code for shielding and protection purposes. Appl Rheology. 2022;32(1):166–77. doi: 10.1515/arh-2022-0132.

[29] El Agammy EF, Mostafa AMA, Al-Zaibani M, Tekin HO, Ramadan R, Essawy AA, et al. 2021). Tailoring the structuralism in xBaO·(30–x) Li_2O· $70B_2O_3$ glasses for highly efficient shields of Gamma radiation and neutrons attenuators. Phys Scr 96(12):125308. doi: 10.1088/1402-4896/ac297b.

[30] Ilik E. Effect of heavy rare-earth element oxides on physical, optical and gamma-ray protection abilities of zinc-borate glasses. Appl Phys A. 2022;128(6):1–10. doi: 10.1007/s00339-022-05642-6.

[31] Makishima A, Mackenzie JD. Calculation of bulk modulus, shear modulus and Poisson's ratio of glass. J Non Cryst Solids. 1975;17:147–57. doi: 10.1016/0022-3093(75)90047-2.

[32] Acikgoz A, Demircan G, Yılmaz D, Aktas B, Yalcin S, Yorulmaz N. Structural, mechanical, radiation shielding properties and albedo parameters of alumina borate glasses: Role of CeO_2 and Er_2O_3. Mater Sci Eng B. 2022;276:115519. doi: 10.1016/j.mseb.2021.115519.

[33] Issa SAM, Kumar A, Sayyed MI, Dong MG, Elmahroug Y. Mechanical and gamma-ray shielding properties of TeO_2-ZnO-NiO glasses. Mater Chem Phys. 2018;212:12–20. doi: 10.1016/j.matchemphys.2018.01.058.

[34] Khalaf MA, Ban CC, Ramli M. The constituents, properties and application of heavyweight concrete: A review. Constr Build Mater. 2019;215:73–89. doi: 10.1016/j.conbuildmat.2019.04.146.

[35] Issa SA, Tekin HO, Elsaman R, Kilicoglu O, Saddeek YB, Sayyed MI. Radiation shielding and mechanical properties of Al_2O_3-Na_2O-B_2O_3-Bi_2O_3 glasses using MCNPX Monte Carlo code. Mater Chem Phys. 2019;223:209–19. doi: 10.1016/j.matchemphys.2018.10.064.

[36] Tekin HO, ALMisned G, Rammah YS, Susoy G, Ali FT, Baykal DS, et al. The significant role of WO_3 on high-dense BaO–P_2O_3 glasses: Transmission factors and a comparative investigation using commercial and other types of shields. Appl Phys A. 2022;128(6):1–11. doi: 10.1007/s00339-022-05620-y.

[37] Oruncak B. Gamma-ray shielding properties of Nd_2O_3 added iron-boron-phosphate based composites. Open Chem. 2022;20(1):237–43. doi: 10.1515/chem-2022-0143.

[38] Waheed F, İmamoğlu M, Karpuz N, Ovalıoğlu H. Simulation of neutrons shielding properties for some medical materials. Int J Comput. Exp Sci Eng. 2022;8(1):5–8. doi: 10.22399/ijcesen.1032359.

[39] Boodaghi Malidarre R, Akkurt İ, Gunoglu K, Akyıldırım H. Fast neutrons shielding properties for HAP-Fe_2O_3 composite materials. Int J Comput. Exp Sci Eng. 2021;7(3):143–5. doi: 10.22399/ijcesen.1012039.

[40] Şen Baykal D, Tekin H, Çakırlı Mutlu R. An investigation on radiation shielding properties of borosilicate glass systems. Int J Comput. Exp Sci Eng. 2021;7(2):99–108. doi: 10.22399/ijcesen.960151.

[41] Iskender A. Effective atomic numbers for Fe–Mn alloy using transmission experiment. Chin Phys Lett. 2007;24:2812. doi: 10.1088/0256-307X/24/10/027.